ACS APPLIED MATERIALS & INTERFACES

Research Article

www.acsami.org

Nanoscale Electrostructural Characterization of Compositionally Graded $Al_xGa_{1-x}N$ Heterostructures on GaN/Sapphire (0001) Substrate

Andrian V. Kuchuk,[*,†,‡] Petro M. Lytvyn,[‡] Chen Li,[†] Hryhorii V. Stanchu,[‡] Yuriy I. Mazur,[†] Morgan E. Ware,[†] Mourad Benamara,[†] Renata Ratajczak,[§] Vitaliy Dorogan,[†] Vasyl P. Kladko,[‡] Alexander E. Belyaev,[‡] and Gregory G. Salamo[†]

[†]Institute for Nanoscience and Engineering, University of Arkansas, West Dickson 731, Fayetteville, Arkansas 72701, United States

[‡]V. Lashkaryov Institute of Semiconductor Physics, National Academy of Sciences of Ukraine, Pr. Nauky 41, 03680 Kyiv, Ukraine

[§]National Centre for Nuclear Research, ul. Andrzeja Sołtana 7, 05-400 Otwock, Poland

Supporting Information

ABSTRACT: We report on $Al_xGa_{1-x}N$ heterostructures resulting from the coherent growth of a positive then a negative gradient of the Al concentration on a [0001]-oriented GaN substrate. These polarization-doped $p-n$ junction structures were characterized at the nanoscale by a combination of averaging as well as depth-resolved experimental techniques including: cross-sectional transmission electron microscopy, high-resolution X-ray diffraction, Rutherford backscattering spectrometry, and scanning probe microscopy. We observed that a small miscut in the substrate orientation along with the accumulated strain during growth led to a change in the mosaic structure of the $Al_xGa_{1-x}N$ film, resulting in the formation of macrosteps on the surface. Moreover, we found a lateral modulation of charge carriers on the surface which were directly correlated with these steps. Finally, using nanoscale probes of the charge density in cross sections of the samples, we have directly measured, semiquantitatively, both n- and p-type polarization doping resulting from the gradient concentration of the $Al_xGa_{1-x}N$ layers.

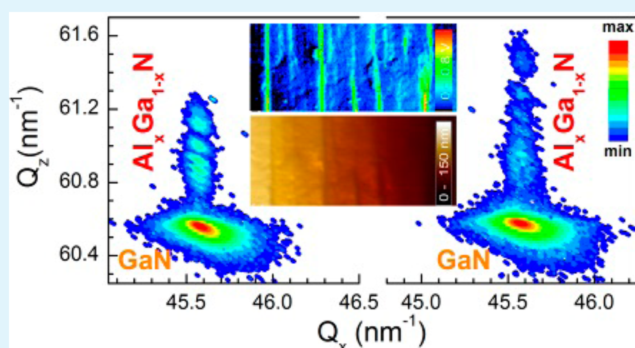

KEYWORDS: *$Al_xGa_{1-x}N$, graded layers, polarization doping, step-bunching effect, threading dislocations, charge accumulation*

1. INTRODUCTION

Compositionally graded $Al_xGa_{1-x}N$ films have recently become very interesting as a result of their potential to enhance p-type doping due to the so-called polarization doping effect.[1] The advantage of this has been demonstrated through devices such as deep-ultraviolet light-emitting diodes,[2,3] lasers,[4] and $p-n$ junctions.[5] Additionally, strain accumulation in these graded films has been shown to incline threading dislocations (TDs), allowing them to annihilate with each other, resulting in the growth of high quality GaN layers.[6,7] The depth profile of the Al concentration determines much of the properties of these graded $Al_xGa_{1-x}N$ layers. Additionally, the influence of the layer thickness on polarization-induced doping and the properties of the resulting 3-dimensional electron slab (3DES) have been determined.[8] However, in all previous studies, the polarization-induced doping results from the compositional grading of Al from $x_{Al} = 0 \rightarrow x_{Al} = 10-30\%$. In a previous work,[9] we showed the possibility of growing graded $Al_xGa_{1-x}N$ coherently strained to the GaN substrate with starting Al concentrations of $x_{Al} > 0\%$, creating an additional way for tuning the polarization-induced doping carrier densities in graded $Al_xGa_{1-x}N$ layers. Indeed, growth of graded $Al_xGa_{1-x}N$ coherently strained to GaN starting with an Al concentration, $x_{Al} > 0\%$, can modify the strain profile due to the lattice mismatch at the interface. Consequently, this changes the piezoelectric component of the polarization, resulting in a similar change to the carrier concentration. Moreover, when the starting Al concentration exceeds a critical value a polarization-induced 2-dimensional electron gas (2DEG) at the $Al_xGa_{1-x}N$/GaN interface can be created. This can be used to realize a new approach for the fabrication of ultralow resistance nonalloyed ohmic contacts for GaN-based transistors.[10] The grading of the Al composition from the channel layer (2DEG) to the heavily doped (n^+-GaN) ohmic layer eliminates abrupt heterojunction band offsets and creates a direct 3D-to-2D contact.

Coherent growth of $Al_xGa_{1-x}N$ layers on GaN results in tensile stress. Depending on the Al concentration and the layer thickness, stress relaxation may occur during deposition to

Received: August 26, 2015
Accepted: October 2, 2015
Published: October 2, 2015

ACS Publications © 2015 American Chemical Society

DOI: 10.1021/acsami.5b07924
ACS Appl. Mater. Interfaces 2015, 7, 23320−23327

partially relieve the accumulated strain by plastic deformation (cracks, dislocations), resulting in noncoherent growth. For fixed composition $Al_xGa_{1-x}N$ layers, the critical thickness for this strain relaxation in $Al_xGa_{1-x}N$/GaN heterostructures has been demonstrated for a wide range of x_{Al}.[11,12] The critical thickness has been measured to be ~100 nm for nongraded $Al_xGa_{1-x}N$ with x_{Al} ~ 14%,[12] which has been the typical thickness of graded $Al_xGa_{1-x}N$ from previous studies.[1−8] For graded $Al_xGa_{1-x}N$ layers, however, there is no similar data regarding the critical thickness for relaxation in the literature. Moreover, for graded $Al_xGa_{1-x}N$ starting with Al concentrations of $x_{Al} > 0\%$, the strain accumulation is larger leading to smaller critical thicknesses. Consequently, in order to exploit such polarization engineered structures a deeper understanding of these strains is necessary.

In this study, we have investigated ~200 nm thick $Al_xGa_{1-x}N$ heterostructures (HS) with Al concentration increasing from x_{Al} ~ 7% to x_{Al} ~ 20−30% at the center of the structure then decreasing back to x_{Al} ~ 7%, with the whole structure coherently strained to the [0001]-oriented GaN template. We first evaluate the structural quality of the active layer by high-resolution X-ray diffraction (HRXRD), transmission electron microscopy (TEM), Rutherford backscattering spectrometry (RBS), and atomic force microscopy (AFM) and correlate the results with the Al content. Finally, charge sensing scanning probe microscopy (SPM) techniques are applied to correlate structural properties with the related localized charge type and density in the $Al_xGa_{1-x}N$ HS.

2. EXPERIMENTAL DETAILS

Crystal growth of $Al_xGa_{1-x}N$ in this work was performed in a Veeco Gen-II plasma-assisted molecular beam epitaxy (PAMBE) system. The samples were grown on substrates from KYMA Technologies consisting of ~5 μm of [0001] oriented GaN grown on AlN/sapphire by hydride vapor phase epitaxy (HVPE). The substrates were first heat cleaned at 700 °C for 1 h in order to remove any residual surface contaminations. Then, a 240 nm thick Ga-polar, undoped GaN buffer layer was grown under gallium-rich conditions and a substrate temperature of 690 °C. Finally, the $Al_xGa_{1-x}N$ layers were grown with the substrate at a temperature of 710 °C under Ga-rich conditions by linearly changing the temperature of the Al effusion cell based on the calibration reported in our previous work.[9] For sample G1 (x_{Al}^{max} = 22%) the Al cell temperature, T_{Al}, was ramped from 957 to 1005.5 °C over 25 min and then immediately decreased over another 25 min. For sample G2 (x_{Al}^{max} = 32%) the same procedure was done, keeping the same starting Al cell temperature but changing the maximum to T_{Al} = 1026 °C.

The structural properties of the as-grown samples were characterized as follows: (1) HRXRD was performed using a Philips X'pert MRD equipped with a standard four-bounce Ge(220) monochromator on the 1.6 kW Cu Kα_1 X-ray tube with vertical line focus and a three bounce (022) channel cut Ge analyzer crystal. (2) RBS measurements were performed using the NEC Pelletron Accelerator (3SDH-2 Pelletron) at the Laboratory for Ion Beam Techniques (ITE-IFPAN, Warsaw, Poland) with a collimated (1.5 mm^2) 2 MeV He^+ beam. The backscattered ions were detected at an angle of 170° to the incidence direction with a Si surface barrier detector with an active area of 50 mm^2. (3) Cross-section transmission electron microscopy (TEM) studies were conducted in an FEI Titan 80−300 TEM equipped with Schottky FEG operated at 300 kV and an EDS detector for elemental analysis. Finally (4) SPM measurements were carried out using a NanoScope IIIa Dimension 3000 scanning probe microscope using ultrasharp silicon tips with additional PtIr coating for electrostatic measurements. Surface potential and charge density mapping was performed at the nanoscale by Kelvin probe force microscopy (KPFM) and electrostatic force gradient microscopy (EFGM).

3. RESULTS AND DISCUSSION

First, in order to accurately determine the strain state and depth profiles of the Al concentration (x_{Al}) in the $Al_xGa_{1-x}N$ HS, we use HRXRD. Figure 1 shows the HRXRD reciprocal space map (RSM) for the asymmetrical ($20\bar{2}5$) reflection of both samples G1 and G2.

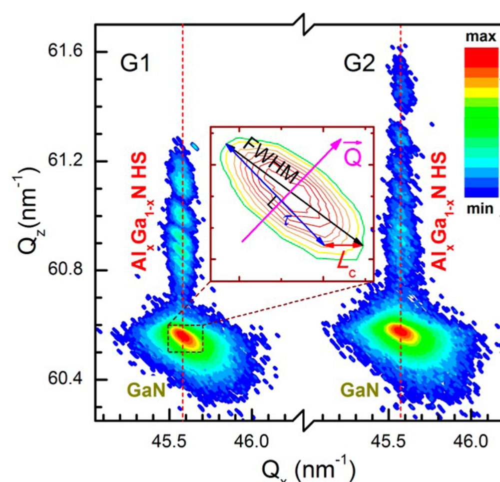

Figure 1. ($20\bar{2}5$) RSMs of graded $Al_xGa_{1-x}N$ HS on GaN for samples G1 and G2. The inset illustrates the influence of lateral coherence length (L_c) and tilt (τ) on broadening the peak comparative to the diffraction vector (Q). Q_z and Q_x are the components of Q.

Here, we see that the peaks from the $Al_xGa_{1-x}N$ HS are vertically aligned with the GaN substrate, indicated by the red vertical dashed lines. This demonstrates that the $Al_xGa_{1-x}N$ HS is fully strained on and coherent with the GaN for both samples G1 and G2 with the same in-plane lattice parameters (a_{HS} = a_{GaN} ~ 0.3184 nm). Thus, the distribution of x_{Al} along the growth direction (c-axis direction) of the graded film affects only the out-of-plane lattice parameter (c_{HS}). To find the variation in c_{HS} throughout the thickness of the $Al_xGa_{1-x}N$ layer we measured the symmetric (0002) RSMs and simulated the extracted $2\theta/\omega$-scans. This is shown in Figure 2 for sample G2 (see Figure S1 in Supporting Information for sample G1).

Here, the back pane shows both the simulated $2\theta/\omega$-scan and the extracted one which was taken from the RSM in the bottom pane at a ω value where the peaks are maximized. For the simulations a kinematical approach assuming epitaxial compositionally graded layers was used.[9] In addition, assuming biaxial strain and Vegard's law, we calculated the depth profiles of the Al concentration by using the in-plane lattice constant a_{HS} and the distribution function of c_{HS} shown in Figure 2 (inset). As seen in Figure 3a, the Al concentration profiles are Λ-shaped as expected from the growth. The concentration, x_{Al}, changes nearly linearly from 7.5% to x_{Al}^{max} = 22(32)% over ~90 nm and back to 7.5% over ~90 nm for G1(G2). The good fit of

DOI: 10.1021/acsami.5b07924
ACS Appl. Mater. Interfaces 2015, 7, 23320−23327

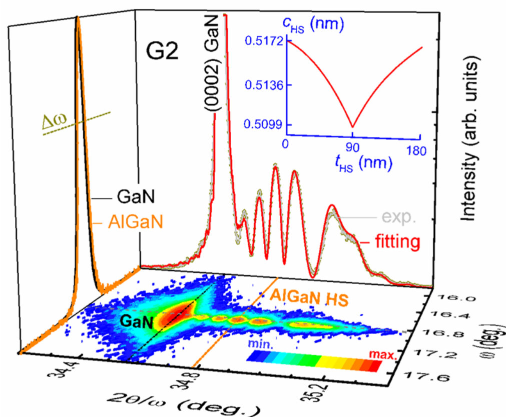

Figure 2. (0002) RSM (bottom) and extracted scans of ω (left) and $2\theta/\omega$ (right) for graded $Al_xGa_{1-x}N$ HS (G2) on GaN. The inset presents the results of $2\theta/\omega$-scan fitting for the out-of-plane lattice parameter c_{HS} distribution as functions of thickness in the graded $Al_xGa_{1-x}N$ HS.

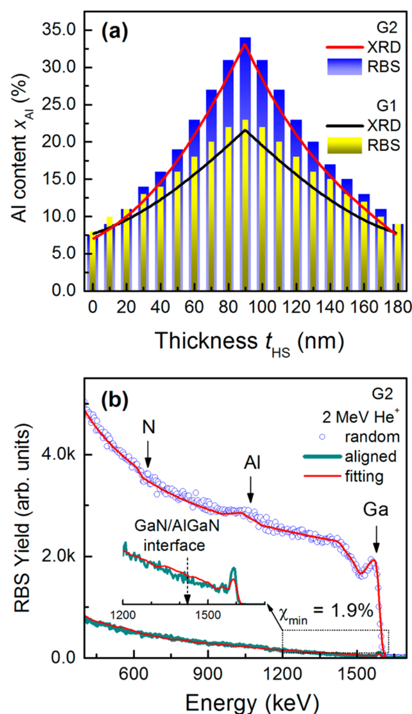

Figure 3. (a) Al concentration depth profiles for samples G1 and G2 (extracted from XRD (line) and RBS (column) measurements). (b) Random and [0001]-aligned RBS/c spectra for the graded $Al_xGa_{1-x}N$ HS G2. Solid (red) lines represent the fitted curves. The arrows (black) indicate the energy of backscattered He^+ ions by film atoms.

the simulation with the $2\theta/\omega$-scans (Figure 2) indicates the high accuracy of the Al concentration profiles, whereas the precision of the in-plane lattice constant, a_{HS}, determines the accuracy of the composition/strain profiles. Additionally, RBS was used to determine the distribution of Al in the graded layers. This technique can provide a measurement of the compositional profiles with depth resolution of a few nanometers independent of lattice strain. Moreover, performing RBS in channeling mode (RBS/c) can give additional information about structural properties. RBS/c spectra were analyzed using the Monte Carlo simulation computer code *McChasy*.[13,14] The random and [0001] channeled RBS spectra for sample G2 are shown in Figure 3b (see Figure S2 in Supporting Information for sample G1). The high energy range (>1500 keV) corresponds to scattering off of Ga atoms. The signal from Al (∼1000 keV) is very weak and overlaps with Ga due to the lighter mass. However, the Al content can be determined indirectly by the deficiency of Ga at a given depth assuming the correct stoichiometry of nitrides, i.e., N content of 50 at. %.[15] It should be noted that, in comparison with the wide area integral analysis from HRXRD, RBS is a very local method. Furthermore, HRXRD and RBS spectra were simulated with a depth resolution of ∼0.5 and ∼10 nm, respectively. Thus, a slight discrepancy between HRXRD and RBS data should be expected. The results of the Al concentration estimate resulting from the random RBS spectra simulation are shown in Figure 3a as the columns. A very good correlation between Al depth profiles estimated by HRXRD and RBS measurements was obtained for both samples.

The structural quality of the graded $Al_xGa_{1-x}N$ HS was evaluated from the ratio between random and channeled backscattering yields in RBS/c, i.e., the minimum backscattering yield, χ_{min}. Low values of χ_{min} (2−5%) indicate a high crystal quality.[15] For our samples we have χ_{min} = 1.6% and χ_{min} = 1.9% for G1 and G2, respectively. The absence of any obvious feature from Al in the channeled spectra is a direct result of the homogeneity of the layers and the perfect AlGaN/GaN interfaces. Thus, HRXRD and RBS/c agree on the quality of the pseudomorphic growth.

A more detailed study of structural properties of graded $Al_xGa_{1-x}N$ HS was performed by further analysis of HRXRD, cross-sectional TEM, and AFM surface morphology. Epitaxial III-nitride films are usually described by a mosaic model, which assumes that the film consists of tilted (with respect to the substrate normal) and twisted (about the substrate normal) mosaic blocks.[16−18] The range of orientation of the mosaic blocks with respect to each other, as well as their coherence lengths, affect the full width at half-maximum (fwhm) of the reflected spots in the RSM as is shown in the inset of Figure 1. Here, the lateral coherence length (L_c) and tilt (τ) broaden the spot in the asymmetrical RSM in directions inclined to each other; i.e., the contribution from L_c is parallel to the surface plane (along the Q_x component of diffraction vector Q), whereas the contribution of τ is normal to Q.[16] As can be seen from Table 1, the extracted parameters of mosaicity for $Al_xGa_{1-x}N$ HS layers differ from that of the GaN substrate.

Table 1. Structural Parameters of G1 and G2 Samples Obtained from the HRXRD Data

		(20$\bar{2}$5) RSMs		(0002) RSMs	
sample	layers	L_c (nm)	τ (arcsec)	$\Delta\omega$ (arcsec)	N_s ($\times 10^8$ cm^{-2})
G1	AlGaN-HS	227 ± 34	173 ± 7	258	1.35
	$GaN_{templ.}$	173 ± 16	150 ± 7	264	1.4
G2	AlGaN-HS	176 ± 22	162 ± 16	321	2.1
	$GaN_{templ.}$	118 ± 8	117 ± 5	317	2

Since the L_c corresponds to the mean distance between TDs, increasing of L_c indicates an improvement of structural quality of the HS layers for both samples. However, at the same time, increasing τ indicates an increase in the distribution of the orientations between HS mosaic blocks. These changes are more significant for sample G2, for which the Al concentration

DOI: 10.1021/acsami.5b07924
ACS Appl. Mater. Interfaces 2015, 7, 23320−23327

is higher. It should be noted that the line widths ($\Delta\omega$) of the (0002) rocking curves for the $Al_xGa_{1-x}N$ HS and the GaN substrate extracted from RSMs (see Figure 2, left side panel) are not significantly different for both samples; i.e., the mosaicity is the same in the film as the substrate.

There are three kinds of TDs present in $Al_xGa_{1-x}N$ HS epilayers and GaN template layers: screw, edge, and mixed.[19,20] The pure screw-type TD has a Burger's vector, $|\boldsymbol{b}_s| = c$, in the [0001] direction. The pure edge-type TD has a Burger's vector, $|\boldsymbol{b}_e| = 1/3 \times a$, in the $[11\bar{2}0]$ direction. And, the mixed-type TD has a Burger's vector, $|\boldsymbol{b}_m|^2 = (1/3 \times a)^2 + c^2$, in the $[11\bar{2}3]$ direction. Thus, the different XRD reflections are sensitive to various types of TDs.[19] The pure screw and screw component of mixed TDs cause the broadening of the symmetric reflections, while the edge-type TDs affect them very little. Therefore, by using the equation $N_s = \Delta\omega^2_{(0002)}/(4.35 \times |\boldsymbol{b}_s|^2)$ we calculate the density of screw-type TDs. As can be seen from Table 1, there is not much difference between the density of screw-type TDs for $Al_xGa_{1-x}N$ HS and GaN substrate. For both samples we find a range of $N_s = 1 \div 2 \times 10^8$ cm^{-2}, which is typical for GaN templates and epitaxial layers.[20] As a result, we conclude that the main source of TDs in the HS is the GaN substrate. To investigate this further, cross-sectional TEM was employed to examine the structural quality of the $Al_xGa_{1-x}N$ HS epilayers and the HS/GaN interface. Figure 4a shows a dark-field image taken under 2-beam conditions with $(1\bar{1}02)$ reflecting planes of the sample G2. These conditions make most dislocations visible independent of their nature. This image shows that the growth of the $Al_xGa_{1-x}N$ HS thin epilayers on top of the GaN template does not interfere with the propagation of TDs. Furthermore, these Al-graded layers do not introduce additional defects. This is confirmed also by observation of the interface between HS epilayers and GaN at higher magnification. The resulting HRTEM image is shown in Figure 4b. This image shows that due to the coherent growth of the graded $Al_xGa_{1-x}N$ HS on GaN the interface is atomically flat and that good epitaxial growth occurred for both G1 and G2 samples. Thus, in spite of starting the HS with an Al concentration of $x_{Al} = 7.5\%$ (corresponding to ~0.2% in-plane lattice mismatch with GaN), the main structural imperfections in the $Al_xGa_{1-x}N$ HS layers are only those TDs which originate in the underlying GaN substrate.

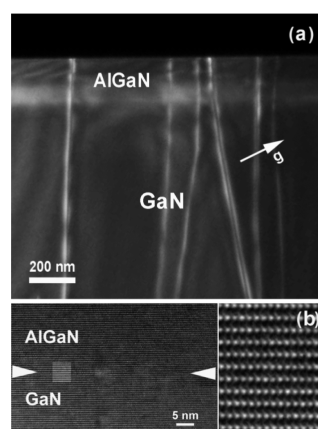

Figure 4. (a) DF image taken under 2-beam condition with $g = [1\bar{1}02]$ showing that $Al_xGa_{1-x}N$ HS (G2) layers do not introduce additional dislocations. (b) HRTEM image along $[1\bar{1}20]$ of the interface between the graded $Al_xGa_{1-x}N$ layer (G2) and the GaN template.

In order to evaluate the morphology of the $Al_xGa_{1-x}N$ films at different growth stages, AFM measurements were performed. The surface of the buffer is typical for films grown in step-flow mode with terrace height and width of ~0.5 and ~130 nm, respectively (Figure 5e). This height is almost the same as the two bilayer steps of GaN ($c = 2 \times 0.259$ nm = 0.518 nm) and corresponds to an epitaxial misorientation (step angle) of $\alpha \sim 0.22°$. In order to confirm the misorientation of the GaN buffer and the crystallographic tilt between the GaN and the sapphire c-axes, as well as their directions, HRXRD $2\theta/\omega$-scans as a function of sample rotation were measured.

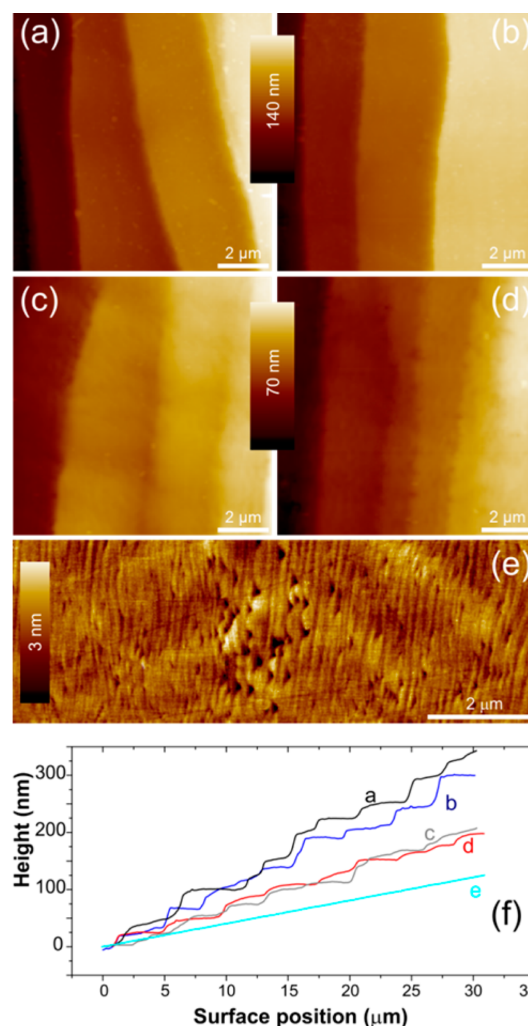

Figure 5. AFM images of as-grown $Al_xGa_{1-x}N$ films: samples with x_{Al}^{max} = 22% (a) and 32% (b) after growth of the positively graded film, i.e., at the half thickness of structures and surfaces of final G1(c) and G2(d) structures. Surface of GaN template shown in (e). Corresponding height profiles of samples illustrated in (f).

The sapphire substrates revealed miscuts of $1.1 \pm 0.1°$ toward the $[1\bar{2}10]$ direction, resulting in the GaN layer misorientation of $\alpha \sim 0.22°$ toward the $[1\bar{1}00]$ direction. This tilt between GaN and sapphire can be explained by the extended Nagai theory.[21] Note the V-shaped pits that are clearly detected on the surface are the result of holes decorating the TDs which are terminated on the surface and which pin the propagation of steps in the step-flow growth regime.

Following from Figure 5a and b the deposition of the 90 nm thick graded $Al_xGa_{1-x}N$ film dramatically alters the surface

DOI: 10.1021/acsami.5b07924
ACS Appl. Mater. Interfaces 2015, 7, 23320−23327

morphology of the crystal. Macrosteps appear due to step bunching on the surface of both the x_{Al}^{max} = 22 and 32% films with heights of 31 and 43 nm, respectively. The typical width of the terraces is the same for both films (~3.0 μm). The heights of the macrosteps decrease by a factor of 2 after further deposition of the 90 nm reverse graded $Al_xGa_{1-x}N$ film (15 and 20 nm for samples G1 and G2, respectively). Whereas the GaN buffer layer was found to have a misorientation angle, $\alpha \sim 0.22°$, toward the $[1\bar{1}00]$ direction, the first 90 nm deposition of the graded layers resulted in larger values of α of 0.6° and 0.8° for the x_{Al}^{max} = 22 and 32% films, respectively. Then, the second 90 nm deposition reduced α to 0.3° and 0.4° in samples G1 and G2, respectively. Typical height profiles across the terraces are shown in Figure 5f. Thus, AFM results reveal that step-bunching results from growing the strained material on vicinal substrates which is well described by surface diffusion and the Ehrlich−Schwoebel effect.[22,23] See Figure S3 in the Supporting Information for a diagram of the strain in the as-grown layers. If the diffusion lengths of adatoms are longer than the step terrace width, the Ehrlich−Schwoebel barrier at the step edge promotes step-bunching. Moreover, the strong correlation between the step heights and the surface composition (x_{Al}) also indicates that strain and relaxation are in part responsible for the large step features. Note that step bunching can lead to the lateral modulations of charge carriers and local fluctuations of surface potential along steps, which will be discussed below.

A small feature differs significantly in the G1 and G2 samples. We can clearly see tiny pits along step edges in Figure 5c and d, whereas the step edges are straight in Figure 5a and b. Note that there are no V-shaped pits detected on the investigated surfaces of the 90 nm thick films. It is known that open pits can be observed on a free crystal surface if the surface energy is comparable with the dislocation strain energy.[24] In our case, the surface pits could be made unstable by increasing the surface energy (increasing x_{Al}, i.e., surface strain) and/or terrace width of steps on the growing crystal surface.[25] Thus, tiny pits along step edges can be explained by moved (or inclined) TDs toward [1−100] direction which terminate at macrostep positions on the surface. It should be noted that inclination of TDs was previously proposed as a mechanism to relax compressive stress in $Al_xGa_{1-x}N$ layers but is not reported in tensile layers.[26,27] The tensile strained $Al_xGa_{1-x}N$ grown on an [0001]-oriented GaN substrate can relax by a combination of cracks and interfacial misfit dislocations.[11,12,18,28] Since our $Al_xGa_{1-x}N$ HS is grown coherently on GaN, AFM and TEM measurements do not show any evidence of crack or misfit dislocation formation. Nevertheless, the changes of the L_c and τ mosaic parameters for $Al_xGa_{1-x}N$ HS and the GaN substrate (see Table 1) can be explained by changes in density of dominant edge-type TDs. Indeed, locking and dragging of TDs by macrosteps for AlN and GaN grown on vicinal sapphire (0001) substrates was previously observed.[29,30] Moreover, it was found that the formation and the lateral propagation of the macrosteps play an important role in the reduction of the TD density via interactions between TDs. For graded-$Al_xGa_{1-x}N$ layers this phenomenon should be extensively investigated because apart from the formation of macrosteps here we have the strain field increasing over the thickness of the layers. Therefore, they simultaneously influence both the motion and inclination of TDs.

The structural properties of the $Al_xGa_{1-x}N$ HS were correlated with the local electrical properties at the nanoscale using a charge sensing SPM technique. The two-path KPFM technique allows simultaneous topography and contactless surface potential mapping based on nullifying of the tip−surface electrostatic force by applying an opposite DC potential to the tip.[31] Fixed surface charges on the sample alter the local surface potential and are measured by KPFM. In addition to the (0001) surface KPFM analysis, specially prepared cross sections of samples G1 and G2 were investigated by KPFM as well as a similar EFGM to identify any regions of static electric field build-up distributed across the layers. EFGM visualizes the electrostatic force gradient acting between a probe and a sample due to localized charge, electric potential, and possible tip−surface contact potential difference. It is based on the same principle as KPFM, but the amplitude or phase of the tip oscillation is mapped instead of surface voltages.[32−34]

Figure 6 shows the results for sample G2 which demonstrated a stronger effect than G1. Here, we see that

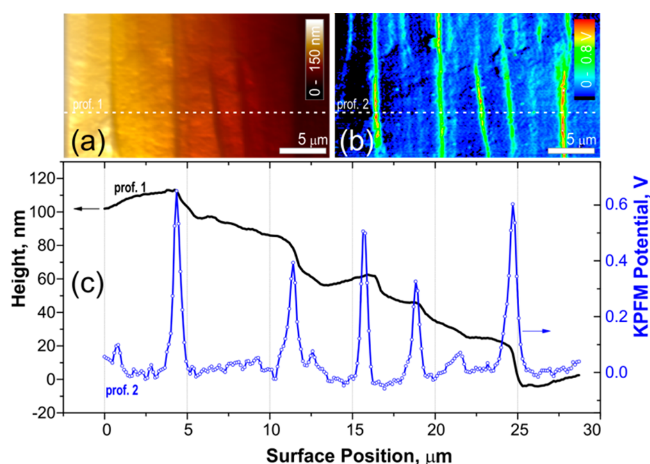

Figure 6. Surface potential fluctuations over the terraces of sample G2. Topography (a), KPFM map (b), and corresponding profiles (c) are shown.

the KPFM measurements (shown in mapping in Figure 6b and in profile in Figure 6c) reveal surface potential variations at the step edges. The potential difference between the surface of the smooth terraces and the macrostep was found to be up to 500 mV (Figure 6c) with the position of the maxima strongly correlating with the step edges. However, there was no strong correlation found between the height of the steps and height of the potential maxima. This indicates that the surface relief has little influence on the KPFM measurements and points to the complex nature of step edge potential. The Kelvin signal can be shown to be proportional to the amount of charge on the surface near the tip. Here, the positive proportionality factor depends only on the tip radius, lift height, and the derivative of the capacitance with respect to the change in height, $\partial C/\partial h$, which is negative. It is custom to show the Kelvin signal as positive for positive surface charge buildup; therefore, the final sign of the proportionality constant is switched. Therefore, our positive KPFM signal indicates a positive charge at the macrostep edges.

It is known that surface steps can form electrostatically confined one-dimensional channels.[35,36] However, this effect is too small to be the only source of the measured maximum potential differences in Figure 6. These large fluctuations are most likely due to the compositional variations during growth at the macrosteps. Indeed, favorable Ga incorporation has been

DOI: 10.1021/acsami.5b07924
ACS Appl. Mater. Interfaces 2015, 7, 23320−23327

found on the side facets of large surface macrosteps.[37,38] These potential variations could additionally be enhanced by a higher density of TDs which have been shown to be concentrated near the step edges and lead to additional charge trapping and some strain relaxation.[29,30] This inhomogeneous dislocation distribution results in inhomogeneous electric characteristics of the $Al_xGa_{1-x}N$ HS.

Graded layers in the investigated samples were detected by KPFM on well-prepared cross sections. The tip geometry and lift height used limit the lateral resolution to ~20 nm. KPFM maps over the samples' cross sections were collected and the signal profiles extracted. Figure 7a shows profiles recorded by

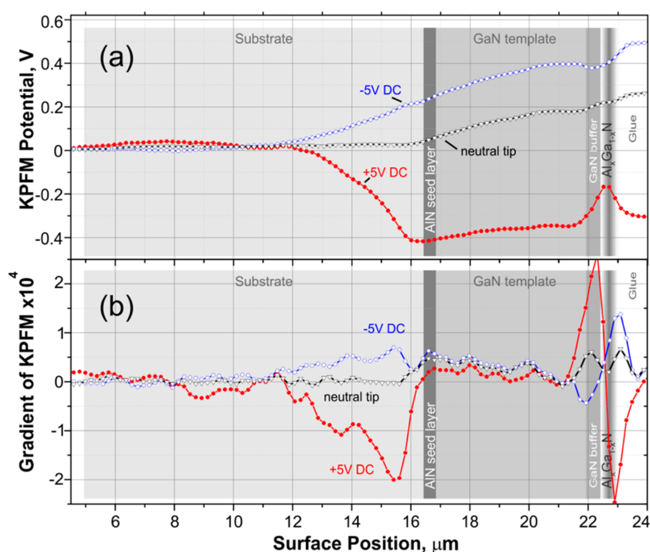

Figure 7. (a) KPFM profiles of the cross-section of sample G2 extracted from corresponding maps (not shown). The data were collected using a neutral tip as well as a tip with +5 and −5 V DC applied bias. (b) Gradients of the measured KPFM surface potential corresponding to the profiles shown in (a). The local gradient of the surface potential illustrates semiquantitatively the sign and density of the free charge. The sample structure is shown in the background of both (a) and (b).

the neutral KPFM tip and with ±5 V additionally applied to the tip. For convenience deep in the sapphire substrate was selected as the reference "0" level for these measurements. The AlN seed layer, the GaN template, and the grown structure show little contrast and are poorly resolved with a neutral tip (curve "neutral tip" in Figure 7a).

Application of an additional voltage to the tip increases the tip−surface electrostatic interaction and the level of the KPFM signal. At the same time, the potential on the tip modifies the surface charges, and the sign of the DC voltage determines the surface polarization. In our case, a negative potential on the tip leads to an increase of positive charges at the surface of the GaN template, and some increasing of the signal is detected over the region of the GaN buffer and the AlGaN layers (curve "−5 V DC"). Monotonic increase of the KPFM signal through the GaN template reflects its inhomogeneous nature. This is most likely directly related to the gradual annihilation of threading dislocations as the material grows thicker because dislocations are known to accumulate static charges along the dislocation line. Inversion of the DC voltage on the tip leads to an inversion of the KPFM signal due to the resulting inverted polarization of the surface (curve "+5 V DC"). For this applied bias we still observe the gradual increase in signal throughout the template region; however, near the surface we find a noticeable signature coinciding with the graded $Al_xGa_{1-x}N$ HS. The sharp change in slope of the curve in the center of the region is a direct result of the polarization doping changing from n-type to p-type by reversing the grade in the $Al_xGa_{1-x}N$ composition. It can be shown that the gradient of this measured local surface potential is proportional to the local density of charge (Figure 7b). As a result, we can see some anomalous concentration of charges in the substrate at the sapphire/AlN interface when a DC voltage is applied to the tip. We can speculate that this is a secondary result of the large charge density within the AlN layer inducing a charge in the subsurface layer of sapphire. Above the AlN, however, there appears to be a uniform decreasing of the charge density continuing through to the top of the GaN template for all curves. This is again consistent with a decreasing density of threading dislocations as the distance from the substrate increases and an unintentionally doped layer is close to the GaN/sapphire interface.[39] Finally, the gradient curves show a sharp increase in charge density in the graded $Al_xGa_{1-x}N$ HS. For the neutral tip we find a symmetrical increase of charge density on either side of the maximum in Al concentration. For this condition there is no determination of charge sign. However, the addition of a DC potential to the tip polarization effects results in large amplitude and asymmetrical maxima which switch polarity at the Al concentration maximum and switch polarity with the sign of the DC voltage. This illustrates a large charge separation by the symmetrical Al-graded layer structure and is a direct measure of both positive and negative charge densities resulting in the positive and negative grade in the Al concentration.

Figure 8 shows the EFGM map and profiles which are derived from the maps by averaging in the vertical direction

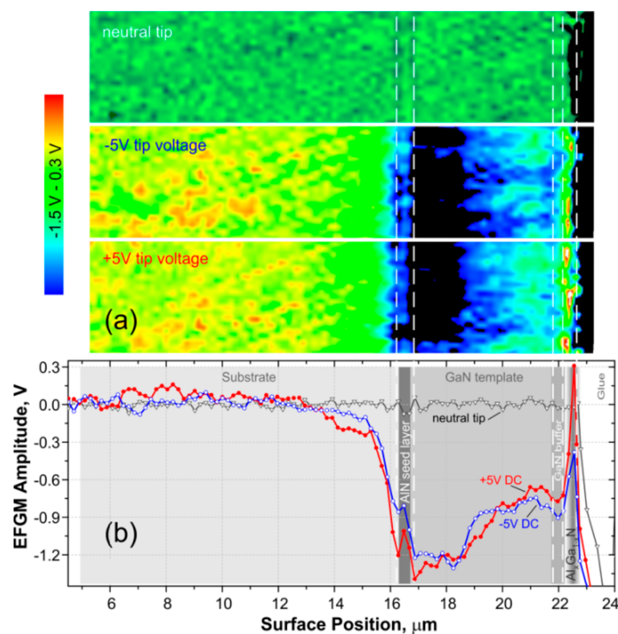

Figure 8. Cross-section mapping of the carrier localization by EFGM on sample G2. Maps are shown in (a), and the corresponding averaged profiles of the EFGM amplitude signal are shown in (b). The maps are collected using a neutral tip and a tip with +5 and −5 V DC applied bias. Scheme of the structure shown in background of (b), and the horizontal scale of (b) applies to both (a) and (b).

DOI: 10.1021/acsami.5b07924
ACS Appl. Mater. Interfaces 2015, 7, 23320−23327

over the total structure of sample G2 starting from within the sapphire substrate up through the graded $Al_xGa_{1-x}N$ layers. EFGM data are independent of the sign of the applied voltage, V, and can be shown to be proportional to V^2.

However, variation in the induced surface charges results in a force differential between the tip and the surface that increases with tip voltage. The EFGM amplitude signal was collected with the tip at a lift height of 20 nm and DC voltages of ±5 V applied between the tip and the substrate surface. If no DC voltage is applied (Figure 8a, top frame), the only contrast is a very weak one from an AlN seed layer which is detected at the interface between the sapphire surface and the base of the GaN template. We find that application of both +5 and −5 V results in a very similar decrease of the EFGM amplitude near the sapphire surface and a slow rise throughout the GaN template layer toward the surface. The highly negative signal amplitude at the base of the template is once more consistent with a significant density of trapped charge on threading dislocations and/or unintentional doping,[40,41] both of which decrease as the density of dislocations decreases throughout the thickness of the GaN template layer as indicated by the decrease in the amplitude of the EFGM signal. After a brief region of stability through the GaN buffer layer, we find a sharp increase in the EFGM amplitude with some instability as it falls off of the surface of the sample measuring an epoxy used to mount the cross-section of the sample. The polarity of the DC voltage on the tip has a significant influence on the EFGM signal amplitude in the area of the $Al_xGa_{1-x}N$ layers which correlates with the KPFM data (Figure 7).

In summary, KPFM and EFGM detect free charge carrier densities in the $Al_xGa_{1-x}N$ HS. The extraordinary macrosteps found on the growth surface act as localization centers for free charge. This could be due to both dislocation pinning and simple field enhancement. However, the EFGM data from the cross sections of our samples indicate that there is a correlation between a high density of dislocations and trapped charge, i.e., close to the substrate both the dislocation density and the observed carrier density are high, and as the film gets thicker there is a reduction in dislocations and a corresponding observation of a reduced charge density. Therefore, we might conclude that the localization of charge on the surface indicates an accumulation of dislocations at the step. This has been observed for thicker GaN growths and is directly related to the miscut of the substrate.[29,30] However, for our samples, the macrosteps appear to be correlated with the strain in the surface material. More study is required to understand what the direct relationship is between polarization doping and defect-related modulation of charge carriers. The accumulation of static charges at macrosteps on the surface and along the dislocation line can lead to some anisotropy in the polarization-induced charge carriers.

4. CONCLUSIONS

Compositionally graded $Al_xGa_{1-x}N$ heterostructures have been grown by PAMBE and their properties probed at the nanoscale. HRXRD, HRTEM, and RBS indicate all HS layers are coherent to the GaN (0001) substrate with the Λ-shaped Al concentration profiles starting from 7.5% to x_{Al}^{max} = 22(32)% over ∼90 nm and back to 7.5% over ∼90 nm. It was found that the vicinal substrate usage and strain accumulation during the growth can enhance the step-flow growth finally leading to the giant step-bunching effect. This leads to changes in the mosaic structure of graded $Al_xGa_{1-x}N$ layers as well as the accumulation of TDs at the step edges. By using KPFM techniques we show that surface macrosteps act as reservoirs for free charge carriers. Additionally, by measuring these samples in the cross-section, we get a direct measurement of the charge density throughout the sample thickness including the GaN template and the graded AlGaN film. A substantial signature of charge accumulation due to threading dislocations throughout the template is apparent and decreases toward the sample surface. Additionally, a direct observation of both electron and hole doping in the graded layers is observed. This is very significant due to the widely observed difficulty in hole doping GaN and even more so $Al_xGa_{1-x}N$.

ASSOCIATED CONTENT

Supporting Information

The Supporting Information is available free of charge on the ACS Publications website at DOI: 10.1021/acsami.5b07924.

(0002) RSMs and extracted scans (ω and $2\theta/\omega$), the out-of-plane lattice parameter c_{HS} distribution as functions of thickness, as well as random and [0001] aligned RBS/c spectra for the graded $Al_xGa_{1-x}N$ HS G1, the strain diagram in the as grown $Al_xGa_{1-x}N$ layers (PDF)

AUTHOR INFORMATION

Corresponding Author

*E-mail: kuchuk@uark.edu. Tel.: +479-445-8818.

Notes

The authors declare no competing financial interest.

ACKNOWLEDGMENTS

The authors acknowledge the financial support of the US National Science Foundation (NSF) via grants no. DMR-1309989, EPSCoR-EPS1003970, and NAS of Ukraine grants no. 27/15H, 19/15H. We thank Dr. K. Pagowska from the Laboratory for Ion Beam Techniques (ITE-IFPAN, Warsaw, Poland) for RBS measurements.

REFERENCES

(1) Simon, J.; Protasenko, V.; Lian, C.; Xing, H.; Jena, D. Polarization-induced Hole Doping in Wide-Band-Gap Uniaxial Semiconductor Heterostructures. *Science* **2010**, *327*, 60−64.

(2) Carnevale, S. D.; Kent, T. F.; Phillips, P. J.; Sarwar, A. T. M. G.; Selcu, C.; Klie, R. F.; Myers, R. C. Mixed Polarity in Polarization-Induced p-n Junction Nanowire Light-Emitting Diodes. *Nano Lett.* **2013**, *13*, 3029−3035.

(3) Verma, J.; Islam, S. M.; Protasenko, V.; Kandaswamy, P. K.; Xing, H.; Jena, D. Tunnel-Injection Quantum Dot Deep-Ultraviolet Light-Emitting Diodes with Polarization-Induced Doping in III-nitride Heterostructures. *Appl. Phys. Lett.* **2014**, *104*, 021105.

(4) Sun, H.; Woodward, J.; Yin, J.; Moldawer, A.; Pecora, E. F.; Nikiforov, A. Yu.; Negro, L.; Paiella, R. Development of AlGaN-based Graded-index-separate-confinement-heterostructure Deep UV Emitters by Molecular Beam Epitaxy. *J. Vac. Sci. Technol. B* **2013**, *31* (3), 03C117.

(5) Li, S.; Ware, M.; Wu, J.; Minor, P.; Wang, Z.; Wu, Z.; Jiang, Y.; Salamo, G. Polarization Induced pn-junction Without Dopant in Graded AlGaN Coherently Strained on GaN. *Appl. Phys. Lett.* **2012**, *101*, 122103.

(6) Li, L.; Yang, L.; Cao, R.; Xu, S. R.; Zhou, X.; Xue, J.; Lin, Z.; Ha, W.; Zhang, J.; Hao, Y. Reduction of Threading Dislocations in N-polar GaN Using a Pseudomorphicaly Grown Graded-Al-fraction AlGaN Interlayer. *J. Cryst. Growth* **2014**, *387*, 1−5.

(7) Yang, Y.; Xiang, P.; Liu, M.; Chen, W.; He, Z.; Han, X.; Ni, Y.; Yang, F.; Yao, Y.; Wu, Z.; Liu, Y.; Zhang, B. Effect of Compositionally Graded AlGaN Buffer Layer Grown by Different Functions of Trimethylaluminum Flow Rates on the Properties of GaN on Si (111) Substrates. *J. Cryst. Growth* **2013**, *376*, 23−27.
(8) Simon, J.; Wang, A.; Xing, H.; Rajan, S.; Jena, D. Carrier Transport and Confinement in Polarization-induced Three-Dimensional Electron Slabs: Importance of Alloy Scattering in AlGaN. *Appl. Phys. Lett.* **2006**, *88*, 042109.
(9) Kuchuk, A. V.; Stanchu, H. V.; Li, C.; Ware, M. E.; Mazur, Yu. I.; Kladko, V. P.; Belyaev, A. E.; Salamo, G. J. Measuring the Depth Profiles of Strain/Composition in AlGaN-Graded Layer by High-Resolution X-ray Diffraction. *J. Appl. Phys.* **2014**, *116*, 224302.
(10) Park, P. S.; Krishnamoorthy, S.; Bajaj, S.; Nath, D. N.; Rajan, S. Recess-Free Nonalloyed Ohmic Contacts on Graded AlGaN Heterojunction FETs. *IEEE Electron Device Lett.* **2015**, *36* (3), 226−228.
(11) Floro, J. A.; Follstaedt, D. M.; Provencio, P.; Hearne, S. J.; Lee, S. R. Misfit Dislocation Formation in the AlGaN/GaN Heterointerface. *J. Appl. Phys.* **2004**, *96*, 7087.
(12) Lee, S. R.; Koleske, D. D.; Cross, K. C.; Floro, J. A.; Waldrip, K. E.; Wise, A. T.; Mahajan, S. *In situ* Measurements of the Critical Thickness for Strain Relaxation in Heterostructures. *Appl. Phys. Lett.* **2004**, *85*, 6164.
(13) Nowicki, L.; Turos, A.; Ratajczak, R.; Stonert, A.; Garrido, F. Modern Analysis of Ion Channeling Data by Monte Carlo Simulations. *Nucl. Instrum. Methods Phys. Res., Sect. B* **2005**, *240*, 277−282.
(14) Turos, A.; Jóźwik, P.; Nowicki, L.; Sathish, N. Ion Channeling Study of Defects in Compound Crystals using Monte Carlo Simulations. *Nucl. Instrum. Methods Phys. Res., Sect. B* **2014**, *332*, 50−55.
(15) Redondo-Cubero, A.; Gago, R.; González-Posada, F.; Kreissig, U.; di Forte Poisson, M.-A.; Braña, A. F.; Muñoz, E. Aluminium Incorporation in $Al_xGa_{1-x}N$/GaN Heterostructures: A Comparative Study by Ion Beam Analysis and X-ray Diffraction. *Thin Solid Films* **2008**, *516*, 8447−8452.
(16) Fewster, P. *X-Ray Scattering from Semiconductors*; Imperial College Press: London, UK, 2003.
(17) Kidd, P. *XRD of Gallium Nitride and Related Compounds: Strain, Composition and Layer Thickness*; Panalytical: Almelo, Netherlands, 2009.
(18) Kladko, V. P.; Kuchuk, A. V.; Lytvyn, P. M.; Yefanov, O. M.; Safriuk, N. V.; Belyaev, A. E.; Mazur, Yu. I.; DeCuir, E. A.; Ware, M. E.; Salamo, G. J. Substrate Effects on the Strain Relaxation in GaN/AlN Short-period Superlattices. *Nanoscale Res. Lett.* **2012**, *7*, 289.
(19) Chierchia, R.; Böttcher, T.; Heinke, H.; Einfeldt, S.; Figge, S.; Hommel, D. Microstructure of Heteroepitaxial GaN Revealed by X-ray Diffraction. *J. Appl. Phys.* **2003**, *93*, 8918.
(20) Zhang, L.; Li, X.; Shao, Y.; Yu, J.; Wu, Y.; Hao, X.; Yin, Z.; Dai, Y.; Tian, Y.; Huo, Q.; Shen, Y.; Hua, Z.; Zhang, B. Improving the Quality of GaN Crystals by Using Graphene or Hexagonal Boron Nitride Nanosheets Substrate. *ACS Appl. Mater. Interfaces* **2015**, *7*, 4504−4510.
(21) Huang, X. R.; Bai, J.; Dudley, M.; Dupuis, R. D.; Chowdhury, U. Epitaxial Tilting of GaN Grown on Vicinal Surfaces of Sapphire. *Appl. Phys. Lett.* **2005**, *86*, 211916.
(22) Ehrlich, G.; Hudda, F. G. Atomic View of Surface Self-Diffusion: Tungsten on Tungsten. *J. Chem. Phys.* **1966**, *44*, 1039−1049.
(23) Schwoebel, R. L.; Shipsey, E. J. Step Motion on Crystal Surfaces. *J. Appl. Phys.* **1966**, *37*, 3682.
(24) Frank, F. C. Capillary Equilibria of Dislocated Crystals. *Acta Crystallogr.* **1951**, *4*, 497−501.
(25) Dalmau, R.; Moody, B.; Schlesser, R.; Mita, S.; Xie, J.; Feneberg, M.; Neuschl, B.; Thonke, K.; Collazo, R.; Rice, A.; Tweedie, J.; Sitar, Z. Growth and Characterization of AlN and AlGaN Epitaxial Films on AlN Single Crystal Substrates. *J. Electrochem. Soc.* **2011**, *158* (5), H530−H535.
(26) Romanov, A. E.; Speck, J. S. Stress Relaxation in Mismatched Layers due to Threading Dislocation Inclination. *Appl. Phys. Lett.* **2003**, *83*, 2569−2571.
(27) Follstaedt, D. M.; Lee, S. R.; Allerman, A. A.; Floro, J. A. Strain Relaxation in AlGaN Multilayer Structures by Inclined Dislocations. *J. Appl. Phys.* **2009**, *105*, 083507.
(28) Einfeldt, S.; Kirchner, V.; Heinke, H.; Dießelberg, M.; Figge, S.; Vogeler, K.; Hommel, D. Strain Relaxation in AlGaN under Tensile Plane Stress. *J. Appl. Phys.* **2000**, *88*, 7029−7036.
(29) Shen, X. Q.; Okumura, H.; Matsuhata, H. Studies of the Annihilation Mechanism of Threading Dislocation in AlN Films Grown on Vicinal Sapphire (0001) Substrates using Transmission Electron Microscopy. *Appl. Phys. Lett.* **2005**, *87*, 101910.
(30) Shen, X. Q.; Okumura, H.; Matsuhata, H. Reduction of the Threading Dislocation Density in GaN Films Grown on Vicinal Sapphire (0001) Substrates. *Appl. Phys. Lett.* **2005**, *86*, 021912.
(31) Nonnenmacher, M.; o'Boyle, M. P.; Wickramasinghe, H. K. Kelvin Probe Force Microscopy. *Appl. Phys. Lett.* **1991**, *58* (25), 2921−2923.
(32) Martin, Y.; Abraham, D. W.; Wickramasinghe, H. K. High-resolution Capacitance Measurement and Potentiometry by Force Microscopy. *Appl. Phys. Lett.* **1988**, *52*, 1103−105.
(33) Terris, B. D.; Stern, J. E.; Rugar, D.; Mamin, H. J. A Localized Charge Force Microscopy. *J. Vac. Sci. Technol., A* **1990**, *8*, 374−377.
(34) Bridger, P. M.; Bandić, Z. Z.; Piquette, E. C.; McGill, T. C. Measurement of Induced Surface Charges, Contact Potentials, and Surface States in GaN by Electric Force Microscopy. *Appl. Phys. Lett.* **1999**, *74* (23), 3522−3524.
(35) Nath, D. N.; Keller, S.; Hsieh, E.; DenBaars, S. P.; Mishra, U. K.; Rajan, S. Lateral Confinement of Electrons in Vicinal N-polar AlGaN/GaN Heterostructure. *Appl. Phys. Lett.* **2010**, *97* (16), 162106.
(36) Li, H.; Zhao, G.; Liu, G.; Wei, H.; Jiao, C.; Yang, S.; Zhu, Q. Study of the One Dimensional Electron Gas Arrays Confined by Steps in Vicinal GaN/AlGaN Heterointerfaces. *J. Appl. Phys.* **2014**, *115* (19), 193704.
(37) Knauer, A.; Zeimer, U.; Kueller, V.; Weyers, M. MOVPE Growth of Al_xGa_1-xN with x ∼ 0.5 on Epitaxial Laterally Overgrown AlN/Sapphire Templates for UV-LEDs. *Phys. Status Solidi C* **2014**, *11* (3−4), 377−380.
(38) Mogilatenko, A.; Küller, V.; Knauer, A.; Jeschke, J.; Zeimer, U.; Weyers, M.; Tränkle, G. Defect Analysis in AlGaN Layers on AlN Templates Obtained by Epitaxial Lateral Overgrowth. *J. Cryst. Growth* **2014**, *402*, 222−229.
(39) Oliver, R. A.; Kappers, M. J.; McAleese, C.; Datta, R.; Sumner, J.; Humphreys, C. J. The Origin and Reduction of Dislocations in Gallium Nitride. *J. Mater. Sci.: Mater. Electron.* **2008**, *19*, S208−S214.
(40) Zhu, T.; Oliver, R. A. Unintentional Doping in GaN. *Phys. Chem. Chem. Phys.* **2012**, *14*, 9558−9573.
(41) Zhernokletov, D. M.; Negara, M. A.; Long, R. D.; Aloni, S.; Nordlund, D.; McIntyre, P. C. Interface Trap Density Reduction for Al_2O_3/GaN (0001) Interfaces by Oxidizing Surface Preparation prior to Atomic Layer Deposition. *ACS Appl. Mater. Interfaces* **2015**, *7* (23), 12774−12780.

DOI: 10.1021/acsami.5b07924
ACS Appl. Mater. Interfaces 2015, 7, 23320−23327